# Bifurcation and Large-Signal Stability Analysis of Three-Phase Voltage Source Converter Under Grid Voltage Dips

Meng Huang, *Member, IEEE*, Yu Peng, Chi K. Tse, *Fellow, IEEE*, Yushuang Liu, Jianjun Sun, *Member, IEEE*, and Xiaoming Zha, *Member, IEEE*

***Abstract*—Three-phase voltage source converters (VSCs) are commonly used as power flow interface in ac/dc hybrid power systems. The ac power grid suffers from unpredictable short-circuit faults and power flow fluctuations, causing undesirable grid voltage dips. The voltage dips may last for a short time or a long duration, and vary the working conditions of VSCs. Due to their nonlinear characteristics, VSCs may enter abnormal operating mode in response to voltage dips. In this paper, the transient response of three-phase VSCs under practical grid voltage dips is studied and a catastrophic bifurcation phenomenon is identified in the system. The converter will exhibit an irreversible instability after the dips. The expanded magnitude of ac reactive current may cause catastrophic consequence for the system. A full-order eigenvalue analysis and a reduced-order mixed-potential-theory-based analysis are adopted to reveal the physical origin of the large-signal instability phenomenon. The key parameters of the system are identified and the boundaries of instability are located. The bifurcation phenomenon and a set of design-oriented stability boundaries in some chosen parameter space are verified by cycle-by-cycle simulations and experimental measurement on a practical grid-connected VSC prototype.**

***Index Terms*—Catastrophic bifurcation, grid voltage dips, large-signal stability, three-phase voltage source converter (VSC), transient response.**

## I. Introduction

With the fast development of renewable energy and microgrid applications, a large amount of renewable energy power generation equipment and user loads are connected to the power grid via power electronic converters. For high power applications, the grid-connected three-phase voltage source converter (VSC) is often used to transmit power bidirectionally between the utility power grid and the energy source or load [1]–[3].

In ac/dc hybrid power systems consisting of converters, renewable sources, loads, and possible storages, transient disturbances are inevitable. The disturbance can be caused by power fluctuations of renewable sources, varying user loads, as well as some unpredictable occurrences of faults in the grid. The faults can be open-circuit or short-circuit faults (single-phase, phase-to-phase or three-phase) and may last for a short time or long duration. As compared to the conventional rotating-machine-based power grid, the power-converter-based power system responds very differently to disturbances. For example, power converters are usually designed with a current control loop that has a wide bandwidth and responds rapidly to the disturbance. Moreover, the feedback control loop would be unstable if the operating point shifts [4]. Furthermore, the sinusoidal pulse width modulation (SPWM) and the equivalent-series-resistance of the components will introduce extra nonlinearities, resulting in abnormal operation of the system [5].

On the other hand, in a practical ac/dc hybrid power system, the grid faults will affect the three-phase VSC in various ways, depending on the fault positions, the configuration of transmission lines, the severity of voltage dips, etc. [6], [7]. The disturbance changes the operating condition of the grid-connected converter dramatically. Therefore, the characteristics of power converters should be thoroughly considered in order to understand the dynamics of such grid-connected systems. Meanwhile, the power grid has some strict requirements for the interface converters. As mentioned in the work of Ma *et al.* [3], the three-phase VSC used in a wind turbine should be connected under various grid voltage dips for a certain time duration. Therefore, it is important to study and characterize the response of VSCs under power grid faults.

Much research effort has been devoted to the characterization of three-phase VSCs around a fixed operating point. In Liserre *et al.* [2], the design and control of an *LCL*-filter-based three-phase active rectifier were studied with an ideal ac source. In Jalili *et al.* [8], the LCL filter design of a three-phase grid-connected converter was studied with emphasis of control consideration. A generalized design procedure of shunt active power

Manuscript received May 29, 2016; revised October 3, 2016 and November 23, 2016; accepted December 27, 2016. Date of publication January 4, 2017; date of current version June 23, 2017. This work was supported in part by the National Natural Science Foundation of China under Grants 51507118, 51637007, and 51190102, and in part by Hong Kong GRF Project PolyU 5258/13E. This paper was presented in part at the *2015 IEEE Energy Conversion Congress and Exposition*, Palais des congrès de Montréal, Montreal, QC, Canada, September 20–24, 2015. Recommended for publication by Associate Editor S. Kapat.

M. Huang, Y. Peng, Y. Liu, J. Sun, and X. Zha are with the School of Electrical Engineering, Wuhan University, Wuhan 430072, China (e-mail: meng.huang@whu.edu.cn; 1039079148@qq.com; 924137340@qq.com; jjsun@whu.edu.cn; xmzha@whu.edu.cn).

C. K. Tse is with the Department of Electronic and Information Engineering, Hong Kong Polytechnic University, Hong Kong (e-mail: michael.tse@polyu.edu.hk).

Color versions of one or more of the figures in this paper are available online at http://ieeexplore.ieee.org.

Digital Object Identifier 10.1109/TPEL.2017.2648119

filters having a similar topology as the three-phase VSC was proposed by Tang *et al.* [9]. All these works were studied under the condition of a sound power grid.

Under practical nonideal power grid conditions, the stability problems were studied previously. In the work of Sun [10], a small-signal method of stability prediction for ac distribution systems was reviewed. An impedance-based small-signal stability criterion of the grid-connected system was proposed [11]. Some research efforts have also been devoted to the fault ride-through capability of VSCs in passive or active approaches. Crowbar protection has been widely used in wind turbine systems as a passive approach to protect the converter during grid faults [12]. In Zamani *et al.* [6], some typical grid faults in an inverter-based microgrid were studied and an enhanced control for the converter with an averaged model was proposed. In Ma *et al.* [3], an unbalanced grid condition was considered, and an effective enhanced control was developed for the unbalanced ac grid. The voltage dips (sags), which are typical grid faults, have been studied from the control point of view. In Junyent-Ferre *et al.* [13], the current control issues were analyzed in detail under unbalanced grid voltage sags. In Miret *et al.* [14], the control scheme for minimizing peak current of three-phase VSC under unbalance grid voltage dips was proposed.

However, most previous studies have focused on the performance improvement aspects of the VSC under the assumption of a sound or faulty power grid. Effective modeling of the nonlinear dynamics of the three-phase VSC under grid faults is often ignored. Moreover, bifurcation analysis has been applied to expose the nonlinear dynamics of the power electronics systems, and in particular, nonlinear stability analysis has been applied to selected power electronics systems, such as parallel-connected boost converter system [15], multistructural photovoltaic-battery hybrid power systems [16], and interconnected power converters [17]. In our previous work [5] and [18], we showed that the three-phase VSC could be driven to exhibit a *catastrophic bifurcation* when operating under disturbance from the dc side or an interacting load from the ac side. In our previous work [5], we considered the disturbance at the dc side of the converter, which is represented by additional capacitive load impedance. The power grid studied in [5] is a sound grid. One difference between a sound grid and a nonideal grid is the way in which the grid voltage is sampled for the converter control. Therefore, the system model and analysis would be different.

Although bifurcation analysis has been found useful for exposing the physical origins of nonlinear behavior and for identifying practical stability regions, its application is generally complex and tedious. Lyapunov-based large signal analysis is a simplified way to examine the system stability under large disturbance, and has been applied to dc–dc, ac–dc, and motor drive systems [19]–[21]. However, there has been very little work on the large-signal stability of grid-connected VSCs under ac side disturbances or faults. Up to now, no large-signal stability criterion has been derived for such systems. This paper attempts to fill this gap.

In our earlier work [22], the bifurcation phenomenon has been identified and a root locus analysis has been performed in terms of a reduced-order system. In this paper, we derive the large-signal stability criterion for the full system, which can be used to determine the stability of the system. Specifically, we consider the three-phase VSC connected to a nonideal power grid under grid voltage dips. In Section II, the dynamic response of an VSC is studied under the grid voltage dips from the ac side. In Section III, a bifurcation analysis is provided to uncover the physical origin of the instability phenomenon. The shifts of the eigenvalues of the full-order system is shown to indicate the instability of the VSC under grid voltage dips. A reduced-order system is applied to expose the catastrophic mechanism of the grid-connected converter system. Moreover, in order to identify the stable operating region, a large-signal stability analysis based on the mixed-potential theory is given and the design-oriented boundaries can be generated. In Section IV, the simulation and experimental results are given to verify the bifurcation and large signal analysis. Section V concludes the paper.

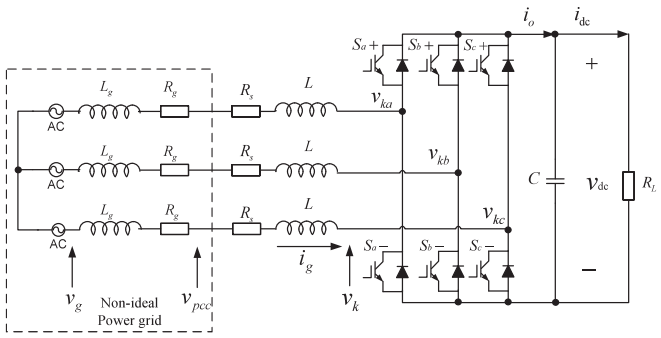


Fig. 1. Three-phase VSC connected to a nonideal power grid.

## II. Glimpse of the Instability

Voltage dips are a kind of grid faults that commonly occur in power grids. A voltage dip appears as a sudden reduction in root-mean-square (rms) value of the ac grid voltage and usually occurs for a short duration. A voltage dip can be caused by a short circuit, excessive loading, or turning ON of electric motors. The rms value of the ac grid voltage may drop by 10% to 90% of its nominal value for several milliseconds or several seconds, and be recovered to its normal value [23], [24]. In practice, power grid faults occurring in any power facility may lead to voltage dips. In general, power grid faults can be classified into two categories, namely, short-circuit faults and broken-line faults. Compared to a broken-line fault, a short-circuit fault may cause more serious damages to the power system. Here, we consider the voltage dips caused by three-phase short-circuit faults that can be a serious fault scenario for the system.

In our study, the power grid is a nonideal power grid that contains grid impedance $L_g$ and $R_g$. The system of a three-phase VSC connected to a nonideal power grid is shown schematically in Fig. 1. The three-phase VSC has a widely used two-level three-wire topology. The six power switches are insulated gate bipolar transistors (IGBTs) operating at 10 kHz. The circuit parameters of the three-phase VSC are summarized in Table I. A commonly used dual-loop control under $dq0$-reference-frame is applied to the VSC, as shown in Fig. 2. The whole system is

TABLE I
CIRCUIT COMPONENT VALUES OF THE THREE-PHASE VSC IN MICROGRID

| Parameters | Value |
|---|---|
| AC grid voltage $V_g$ | 110 $V_{\rm rms}$ |
| AC grid frequency $f_l$ | 50 Hz |
| Grid impedance $L_g$ | 1 mH |
| Grid impedance $R_g$ | 0.2 Ω |
| Rated dc output voltage $V_{\rm dc,ref}$ | 360 V |
| Switching frequency $f_s$ | 20 kHz |
| Filter inductance $L$ | 3 mH |
| Parasitic resistance $R_s$ | 0.1 Ω |
| DC-link capacitor $C$ | 1.5 mF |
| Load resister $R_L$ | 50 Ω |
| DC gain of voltage loop $k_{\rm vp}$ | 2 |
| Integration factor of voltage loop $k_{\rm vp}$ | 100 |
| DC gain of current loop $k_{\rm vp}$ | 10 |
| Integration factor of voltage loop $k_{\rm vp}$ | 200 |

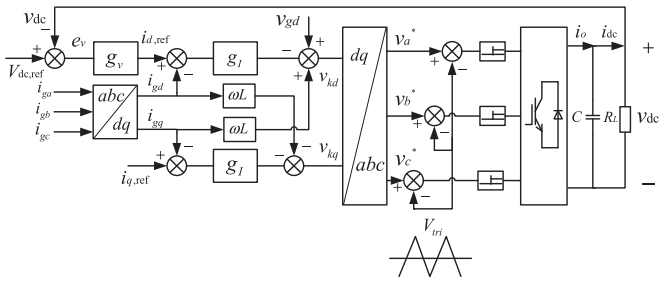


Fig. 2. Dual-loop control of three-phase VSC under $dq$-reference-frame.

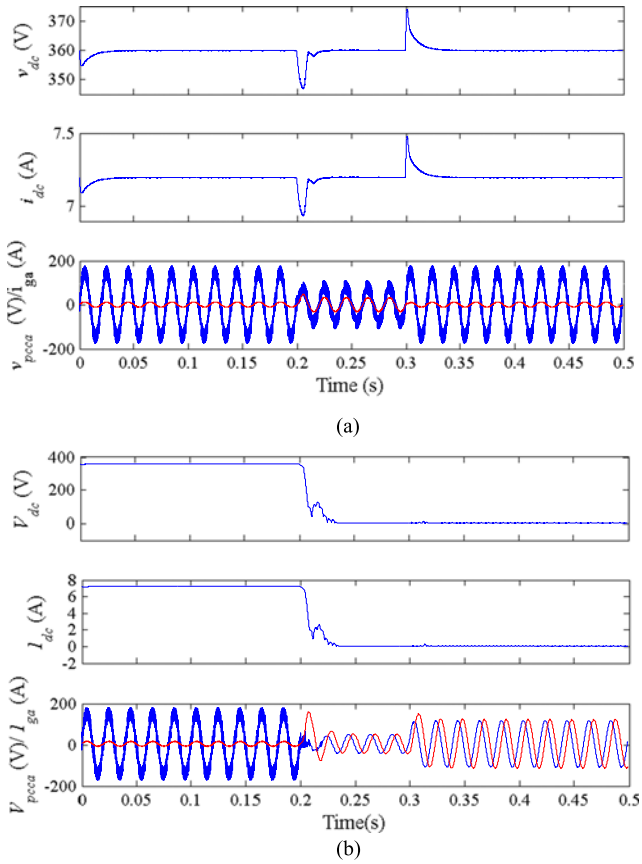


Fig. 3. Transient response of three-phase VSC. (a) Grid voltage drops to 50% of its normal value and lasts for 0.1 s. The fault starts at 0.2 s, and the system steps to a new stable operating point. (b) Grid voltage drops to 45% of its normal value and lasts for 0.1 s. The fault starts at 0.2 s, and the system exhibits a catastrophic bifurcation failing to return to its normal operating mode.

set up for simulation that is performed in MATLAB Simulink with detailed cycle-by-cycle circuit models.

Assuming that the ac grid voltage drops at $t = 0.2$ s in the simulation, Fig. 3 shows the transient response waveform of the operation of the VSC before and after the grid voltage dip occurs. Before $t = 0.2$ s, the three-phase VSC works stably with the ac current regulated at about 8 A. The ac current is in phase with the ac grid voltage. At $t = 0.2$ s, the ac grid is subject to a temporary grid voltage dip.

When the power grid voltage drops abruptly to 50% of its normal value and the fault lasts for 0.1 s, the system remains stable, as shown in Fig. 3(a). The trajectory is represented by the red curve in Fig. 4. However, when the power grid voltage drops abruptly to 45% of its normal value at $t = 0.2$ s, it can be observed that, immediately following the grid voltage dip, the input line current suddenly increases to over 100 A and stays there for the rest of the time. The ac current is no longer in phase with the ac grid voltage, and a large amount of reactive power is drained from the power grid. Meanwhile, the dc output voltage drops to about 45 V and is left unregulated. The six IGBT switches are working in the six-step mode after the fault. This working mode will introduce a high current stress on the IGBT devices. In power electronics systems, the "jump"-type bifurcation phenomenon is usually accompanied by a structural change in the system as some control parameters are varied through the critical point [25], and such a bifurcation may cause undesirable or even catastrophic consequences as the state variables may exhibit undesirably wide excursion in the state space causing damages to some system components. Therefore, this phenomenon, as shown in Fig. 3(b), can be recognized as a kind of catastrophic bifurcation and the system enters an abnormal operating mode [5]. After 0.3 s, the grid voltage recovers to its normal value. However, the phenomenon is irreversible as the converter cannot be restored to its normal operation unless it is restarted manually. The phenomenon is clearly shown in the phase portrait. As shown in Fig. 4 (blue curve), before the occurrence of the voltage dip, the system is working near the operating point. After the voltage dip, the trajectory diverges to infinity or reaches a practical saturation.

In general, border collision bifurcation phenomena widely exist in piecewise-smooth systems [25], [26]. They can be a persistent border-collision type [27], [28], or other more complex forms [29]–[32]. The *catastrophic bifurcation* is a complex border collision bifurcation, which can be understood as a stable equilibrium point colliding with a switching manifold. Specifically, the stable equilibrium point changes suddenly to an unstable one, as triggered by a structural change, which is the topological sequence alternation of the dynamic system. The change is driven by the varying of some parameter across a critical value. Therefore, a *catastrophic bifurcation* can be considered as a qualitative change in the system's behavior, and

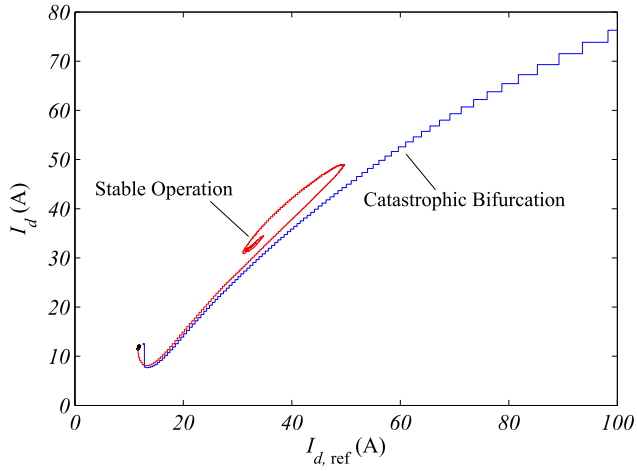


Fig. 4. Trajectory of the system under a grid voltage dip. Red curve: The system returns to a new stable operating point when the disturbance of Fig. 3(a) is applied. Blue curve: A catastrophic bifurcation occurs when the disturbance of Fig. 3(b) is applied.

from a practical viewpoint, the system goes from a stable operation to an unstable one, and no other stable equilibrium or stable limit cycle can be found in its neighborhood [33]. Meanwhile, the system switches to a completely different mode of behavior and collapses abruptly [34].

In the grid-connected converter system under study, we observe that the operation suddenly switches to an unstable mode after a grid voltage dip occurs. The dc output voltage collapses, and a large amount of reactive power emerges at the ac side of the system, possibly causing serious damage to the converter and the grid. The system, thus, exhibits a catastrophic bifurcation that cannot be reversed to its normal state. The phenomenon is not a simple saddle-node bifurcation, but rather a special bifurcation that manifests itself in the phase space as a sudden enlargement of the phase portrait.

## III. Bifurcation Analysis

We now examine the physical origin of the catastrophic bifurcation in this system. First, the eigenvalues of the system are derived to examine the stability of the system around the equilibrium points. Then, the structural change of the system is demonstrated and the mechanism of the catastrophic bifurcation is identified. Furthermore, the large-signal stability is evaluated. We also show that the stable regions can be calculated in a much simpler way using the mixed-potential theory.

### A. Eigenvalues

The switching process of the IGBTs can be modeled by the state-space averaging method. Specifically, the state equations of the three-phase VSC in the stationary $abc$-reference-frame can be written as

$$L\frac{di_{\mathrm{gl}}}{dt} = v_g - (R_g + R_s)i_{\mathrm{gl}} - v_k \tag{1}$$

$$C\frac{dv_{\mathrm{dc}}}{dt} = \sum_{l=a,b,c} i_{\mathrm{gl}} m_l(t) - i_{\mathrm{dc}} \tag{2}$$

where the $i_{\mathrm{gl}}$ is the grid line current with $l = a, b, c$, and the switching function $m_l(t) = \frac{v_k^*}{V_{\mathrm{tri,peak}}}$, with $v_k^*$ being the modulation command and $V_{\mathrm{tri,peak}}$ the peak value of the triangular carrier wave.

Using the Park–Clarke transformation, the three-phase VSC can be modeled in the rotating $dq$-reference-frame, i.e.,

$$L\frac{di_{\mathrm{gd}}}{dt} = \omega L i_{\mathrm{gq}} - (R_g + R_s)i_{\mathrm{gd}} + v_{\mathrm{gd}} - v_{\mathrm{kd}} \tag{3}$$

$$L\frac{di_{\mathrm{gq}}}{dt} = -\omega L i_{\mathrm{gd}} - (R_g + R_s)i_{\mathrm{gq}} + v_{\mathrm{gq}} - v_{\mathrm{kq}} \tag{4}$$

$$C\frac{dv_{\mathrm{dc}}}{dt} = \frac{3}{2v_{\mathrm{dc}}}(v_{\mathrm{kd}} i_{\mathrm{gd}} + v_{\mathrm{kq}} i_{\mathrm{gq}}) - \frac{v_{\mathrm{dc}}}{R_L} \tag{5}$$

where subscripts $d$, $q$ correspond to the standard $d$–$q$ transformed variables; $i_{\mathrm{gd}}$ and $i_{\mathrm{gq}}$ are used to represent the magnitude and phase, respectively, of $i_g$, where $i_g$ is the vector of grid current; and $\omega = 2\pi f_l$ is the angular frequency of the line frequency. Equations (3) and (4) are used in the inner-current loop and (2) is used in the outer-voltage loop. Also, $v_{pccd,q}$ is used to represent the voltage at the point of common coupling in the $dq$-axis.

We define $x_1$, $x_2$, and $x_3$ as internal control variables for convenience of presentation and analysis. Specifically, if a proportional–integral (PI) control is adopted, the control loop can be expressed as

$$\frac{dx_1}{dt} = V_{\mathrm{dc,ref}} - v_{\mathrm{dc}} \tag{6}$$

$$i_{d,\mathrm{ref}} = K_{\mathrm{vp}}(V_{\mathrm{dc,ref}} - v_{\mathrm{dc}}) + K_{\mathrm{vi}} x_1. \tag{7}$$

For the inner current loop, we have

$$\frac{dx_2}{dt} = i_{d,\mathrm{ref}} - i_{\mathrm{gd}} \tag{8}$$

$$\frac{dx_3}{dt} = I_{q,\mathrm{ref}} - i_{\mathrm{gq}} \tag{9}$$

$$v_{\mathrm{kd}} = v_{\mathrm{gd}} - R_g i_d + \frac{L_g}{L} R_s i_d + \frac{L_g + L}{L}(\omega L i_q - k_{\mathrm{ip}}(i_{d,\mathrm{ref}} - i_d) - k_{\mathrm{ii}} x_2) \tag{10}$$

$$v_{\mathrm{kq}} = v_{\mathrm{gq}} - R_g i_q + \frac{L_g}{L} R_s i_q + \frac{L_g + L}{L}(-\omega L i_d - k_{\mathrm{ip}}(I_{q,\mathrm{ref}} - i_q) - k_{\mathrm{ii}} x_3). \tag{11}$$

Here, the reactive power is regulated to zero because $I_{q,\mathrm{ref}}$ is set to zero. The converter and the feedback loop can, thus, be described by state equations (3) through (9) together with control equations (10) and (11).

There are six independent state variables forming the state vector $x = [i_{\mathrm{gd}}\ i_{\mathrm{gq}}\ v_{\mathrm{dc}}\ x_1\ x_2\ x_3]^T$. The input variables can be chosen as $u = [v_{\mathrm{gd}}\ v_{\mathrm{gq}}\ V_{\mathrm{dc,ref}}\ I_{q,\mathrm{ref}}\ R_L]^T$. The state equations are (3)–(5), (7), (10), and (11). However, the control vector $y = [v_{\mathrm{kd}}\ v_{\mathrm{kq}}]^T$ is affected by the nonideal power grid. Therefore, the state equation of the system is expressed as $\dot{x} = f(x, y, u)$, with $y = g(x, u)$, as given in the Appendix.

TABLE II
EIGENVALUE OF GRID-CONNECTED VSC SYSTEM WITH VARYING GRID VOLTAGE

| Voltage dip severity (%) | $v_{\mathrm{pccd}}$ (V) | $i_{d,\mathrm{ref}}$ (A) | Eigenvalues |
|---|---|---|---|
| 100% (Normal grid) | 134.71 | 13.36 | $-1043.0 \pm 778.8i$ |
| 90% | 121.23 | 14.99 | $-924.8 \pm 655.4i$ |
| 80% | 107.77 | 17.12 | $-682.8 \pm 555.4i$ |
| 70% | 94.30 | 20.02 | $-443.1 \pm 649.5i$ |
| 60% | 80.83 | 24.30 | $-260.2 \pm 769.1i$ |
| 50% | 67.36 | 31.57 | $-16.89 \pm 911.9i$ |
| 49% | 66.00 | 32.64 | $17.69 \pm 928.2i$ |
| 40% | 53.88 | 52.65 | $686.1 \pm 1019.1i$ |

By setting the time-derivatives to zero, the equilibrium point $X_Q$ in the $d$–$q$ frame can be readily found, i.e.,

$$X_Q = \begin{cases} I_d = I_{d,\mathrm{ref}} = \dfrac{v_{\mathrm{gd}} - \sqrt{v_{\mathrm{gd}}^2 - \frac{8(R_s+R_g)V_{\mathrm{dc,ref}}^2}{3(R_L)}}}{2(R_s+R_g)} \\ I_q = I_{q,\mathrm{ref}} = 0 \\ V_{\mathrm{dc}} = V_{\mathrm{dc,ref}} \\ x_1 = \frac{I_{d,\mathrm{ref}}}{k_{\mathrm{vi}}} \\ x_2 = \frac{R_s I_{d,\mathrm{ref}}}{k_{\mathrm{vi}}} \\ x_3 = 0. \end{cases} \tag{12}$$

In order to analyze the stability of the system around the equilibrium point, the Jacobian at $X_Q$ is first derived (details given in the Appendix):

$$A = J(X_Q) = \frac{\partial f}{\partial x} + \frac{\partial f}{\partial g}\frac{\partial g}{\partial x}\bigg|_{x=X_Q}. \tag{13}$$

Then, the eigenvalues can be calculated from $\det[\lambda I - A] = 0$. Since the grid voltage is the key parameter affecting the stability, the eigenvalues of the system with different values of grid voltage $v_{\mathrm{gd}}$ are listed in Table II. It can be seen from the movement of the eigenvalues that the system loses its stability when the pair of eigenvalues moves across the imaginary axis under a grid voltage dip, as shown in Fig. 5.

### B. Structural Change Due to Nonlinearities

When the grid voltage dip is more severe, examining the real part of the pair of eigenvalues shows an oscillation of diverging amplitude. The state variables will oscillate with large amplitudes. Therefore, the SPWM module may enter an overmodulation region.

This overmodulation will introduce a nonlinearity to the mechanism that generates the current in the three-phase VSC. As discussed in [5], the phase voltage at the mid-point of the half-bridge switches is

$$v_{\mathrm{kl}} = \frac{v_{\mathrm{dc}}}{2} m_l \tag{14}$$

where $l = a, b, c$ correspond to phases A, B, C, respectively.

When $m_l \leq 1$, the linear relationship of the modulation will satisfy (14), and $v_{\mathrm{kl}}$ can be generated accordingly from the control output. However, when $m_l > 1$, the linearity no longer holds, and $v_{\mathrm{kl}}$ becomes

$$v_{\mathrm{kl}} = \frac{v_{\mathrm{dc}}}{\pi}\left(m_l \sin^{-1}\frac{1}{m_l} + \sqrt{1 - \frac{1}{m_l^2}}\right). \tag{15}$$

In the $dq$-reference-frame, $v_{\mathrm{kd},q}$ will be saturated when $m_l$ is much larger than 1, i.e.,

$$v_{\mathrm{kd,saturated}} = \frac{-(i_{d,\mathrm{ref}} - i_{\mathrm{gd}})}{\sqrt{(i_{d,\mathrm{ref}} - i_{\mathrm{gd}})^2 + i_{\mathrm{gq}}^2}} V_{k,\max} \tag{16}$$

$$v_{kq,\mathrm{saturated}} = \frac{i_{\mathrm{gq}}}{\sqrt{(i_{d,\mathrm{ref}} - i_{\mathrm{gd}})^2 + i_{\mathrm{gq}}^2}} V_{k,\max} \tag{17}$$

where $V_{k,\max} = 2v_{\mathrm{dc}}/\pi$ is the phase voltage when $m_l \gg 1$.

Therefore, the current will saturate when the VSC enters the overmodulation mode. As shown in Fig. 6, the dc output current $i_o$ has a linear relationship with $i_{d,\mathrm{ref}}$ when $i_{d,\mathrm{ref}}$ is small. However, if $i_{d,\mathrm{ref}}$ is driven to a high value, $i_o$ no longer increases linearly, but saturates at a certain value. This is because the practical line current $i_{\mathrm{gd},q}$ would not follow $i_{d,q,\mathrm{ref}}$ due to

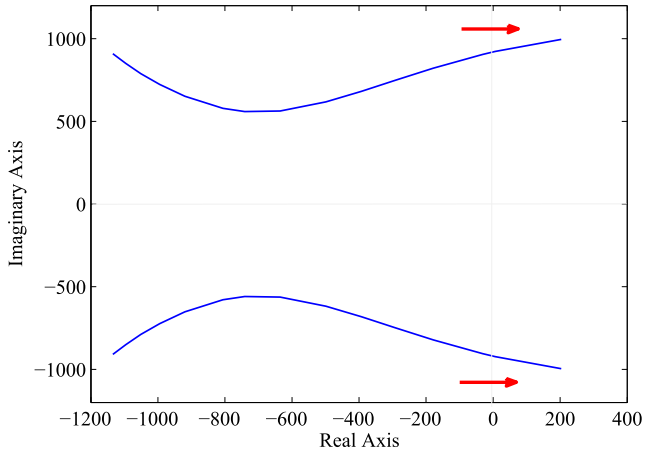


Fig. 5. Pair of the eigenvalues moving from left half-plane to right half-plane.

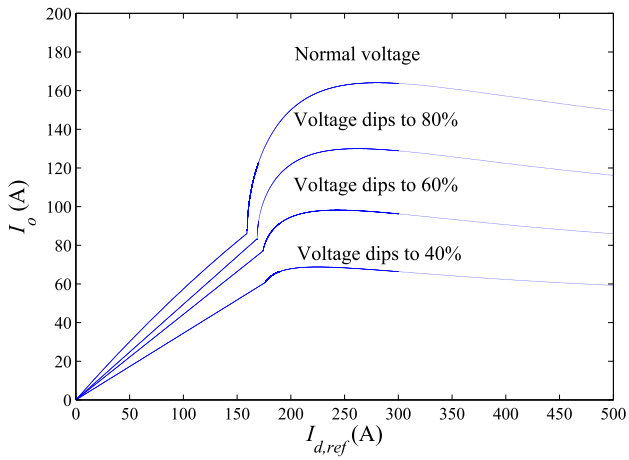


Fig. 6. Saturating nonlinearity of the mechanism that generates the output current.

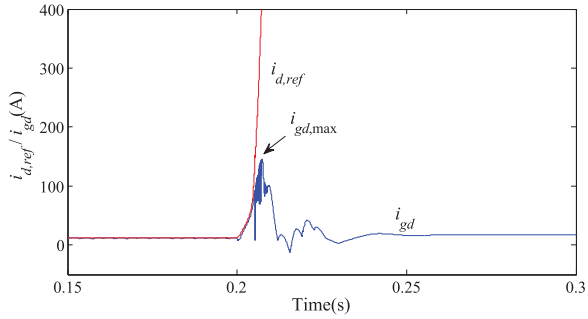


Fig. 7. Reference current $i_{d,\mathrm{ref}}$ versus active current $i_{\mathrm{gd}}$.

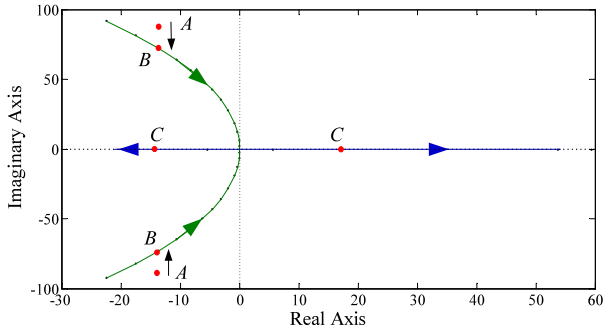


Fig. 8. Root locus of the system when the current gets saturated.

the saturation of the SPWM as well as the power loss in the transmission lines. Considering the nonlinearities, the critical value $i_{d,\mathrm{critical}}$ where $i_{\mathrm{gd}}$ is saturated is

$$i_{d,\mathrm{critical}} = \frac{v_{\mathrm{gd}}R_s + \sqrt{v_{\mathrm{gd}}^2R_s^2 + (R_s^2+\omega^2L^2)(v_{\mathrm{gd}}^2 - V_{k,\max}^2)}}{R_s^2+\omega^2L^2}. \tag{18}$$

The nonlinear current relationship can be expressed as a piecewise function, i.e.,

$$i_{\mathrm{gd}} = f_d(i_{d,\mathrm{ref}}) \tag{19}$$

$$i_{\mathrm{gq}} = f_q(i_{d,\mathrm{ref}}) \tag{20}$$

where

$$f_d(i_{d,\mathrm{ref}}) = \begin{cases} i_{d,\mathrm{ref}}, & \text{if } i_{d,\mathrm{ref}} < i_{d,\mathrm{critical}} \\ h_d(i_{d,\mathrm{ref}}), & \text{if } i_{d,\mathrm{ref}} \geq i_{d,\mathrm{critical}} \end{cases} \tag{21}$$

$$f_q(i_{d,\mathrm{ref}}) = \begin{cases} 0, & \text{if } i_{d,\mathrm{ref}} < i_{d,\mathrm{critical}} \\ h_q(i_{d,\mathrm{ref}}), & \text{if } i_{d,\mathrm{ref}} \geq i_{d,\mathrm{critical}} \end{cases}. \tag{22}$$

The method for calculating $h_{dq}$ can also be found in [5].

The above relationship is clearly evidenced from the transient simulation shown in Fig. 7. The $d$-axis current $i_{\mathrm{gd}}$ cannot follow the reference value $i_{d,\mathrm{ref}}$ after the system hits the bifurcation point and finally saturates at a certain value.

Ignoring the dynamics of the inner current loop, the characteristic equation of the outer voltage loop can be written as

$$\lambda^2 + \frac{3}{2C}\frac{v_{\mathrm{gd}}f_d' - 2R_s(f_df_d' + f_qf_q')}{V_{\mathrm{dc,ref}}}(k_{\mathrm{ip}}\lambda + k_{\mathrm{ii}}) = 0. \tag{23}$$

The roots of the characteristic equation can be found readily by solving (23).

It can be concluded that the system exhibits a structural change when the current gets saturated. A positive real root comes out from the characteristic equation of the outer voltage loop which indicates divergence of the system to infinity or convergence to zero. As shown in Fig. 8, when the grid voltage drops to 40% of its nominal value, the root locus corresponding to the voltage loop moves to point B, and then to point C spontaneously as a result of the control action. It can be concluded that the structure of the system will change at point C, leading to a catastrophic bifurcation. This phenomenon is a typical nonsmooth bifurcation. Since the consequence is a large amount of reactive power being emerged in this system, the phenomenon can be identified as a catastrophic bifurcation of the system under grid voltage dips.

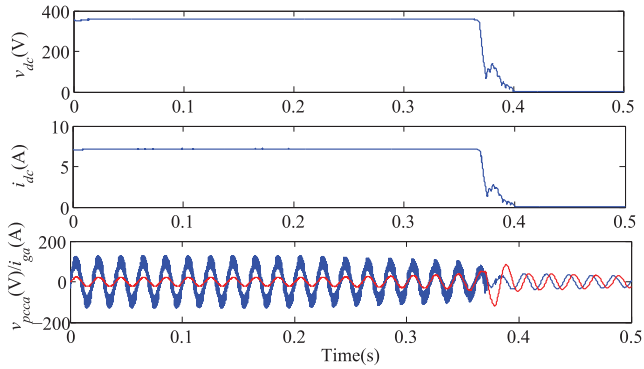


Fig. 9. Transient simulation with grid voltage changed continuously.

Bifurcation analysis is generally performed with the parameter being changed continuously. However, in this system, the transient response to a sudden drop in the grid voltage is similar to a continuous change in the grid voltage because the system will hit the critical point of the $d$-axis current $i_{d,\mathrm{critical}}$. Once the system hits the critical point, it exhibits a catastrophic bifurcation and enters an unstable region. Therefore, the system behaves in the same fashion regardless of how the parameter is changed. A transient simulation with grid voltage changed continuously is shown in Fig. 9. Here, the transient response under a voltage dip is similar to a continuous change in the grid voltage. Thus, the bifurcation analysis is also applicable to the voltage dip scenario studied in this paper.

### C. Stability Analysis and Stable Operating Regions

The local stability of an equilibrium point has been presented in the previous sections. The system is linearized around the equilibrium point but no information is provided about how far away from the equilibrium point the linearization would remain valid. Thus, the global stability which is the stability under large disturbance of the system is still unknown. The grid voltage dip is always a kind of large disturbance for the three-phase VSC.

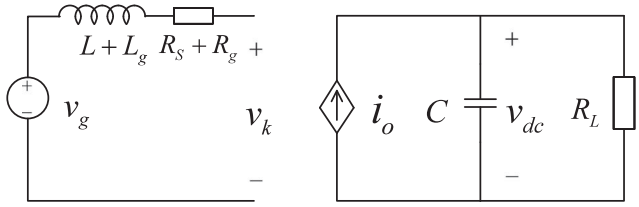


Fig. 10. Simplified model of three-phase VSC with controlled current source.

Therefore, it is essential to examine the global stability of the system.

The above-mentioned bifurcation analysis helps to uncover the physical origin for the loss of stability of a grid-connected three-phase VSC system. However, the system is still quite complex due to multiple bifurcation processes, and the stability boundaries are hard to compute in practice. Here, a Lyapunov-based large signal stability analysis, which is more tractable, is performed. In particular, we adopt the *mixed-potential theory* that gives a Lyapunov function readily and is, thus, an effective approach for large-signal analysis.

The grid-connected three-phase VSC system can be simplified as a controlled current source with a load and a dc-link capacitor, as shown in Fig. 10. In this model, the current source $i_o$ is controlled by the voltage $v_k$. At the stable operating (equilibrium) point, $i_o$ is determined by the active power input of the VSC, i.e.,

$$i_o = \frac{3v_{\rm kd}i_{\rm gd}}{2v_{\rm dc}}. \tag{24}$$

The formulation of the mixed-potential function can be found in [35]. Specifically, since the three-phase grid-connected converter is a boost-type converter, the formulation of the mixed-potential function is similar to that applied to the boost dc–dc converter [19], [36], [37]. Thus, the mixed-potential function of the system can be defined in terms of the vector of inductor currents and the vector of capacitor voltages of the system [35].

Therefore, for the simplified system, the current potential of all the nonstorage elements can be written as (only active power is considered at the equilibrium point)

$$\begin{aligned}\int \sum_{\mu>r+s} v_\mu di_\mu &= \int_0^{i_{\rm gd}} (v_{\rm gd}-v_{\rm kd})di_{\rm gd} \\ &\quad - \int_0^{i_{\rm gd}} (R_g+R_s)i_{\rm gd}di_{\rm gd} + \int_0^{i_o} v_{\rm dc}di_o - \int_0^{\frac{v_{\rm dc}}{R_L}} v_{\rm dc}di_{\rm dc} \\ &= (v_{\rm gd}-v_{\rm kd})i_{\rm gd} - \frac{1}{2}(R_g+R_s)i_{\rm gd}^2 + v_{\rm dc}i_o \\ &\quad - \int_0^{v_{\rm dc}} i_o dv_{\rm dc} - \frac{v_{\rm dc}^2}{2R_L}. \end{aligned} \tag{25}$$

The sum of energy on the capacitors is

$$\sum_{\delta=r+1}^{r+s} i_\delta v_\delta = -\left(i_o - \frac{v_{\rm dc}}{R_L}\right)v_{\rm dc} = -v_{\rm dc}i_o + \frac{v_{\rm dc}^2}{R_L}. \tag{26}$$

Therefore, the mixed-potential function, which is also a Lyapunov function, can be obtained as

$$\begin{aligned} P(i,v) &= \int \sum_{\mu>r+s} v_\mu di_\mu + \sum_{\delta=r+1}^{r+s} i_\delta v_\delta \\ &= (v_{\rm gd}-v_{\rm kd})i_{\rm gd} - \frac{(R_g+R_s)i_{\rm gd}^2}{2} \\ &\quad - \int_0^{v_{\rm dc}} i_o dv_{\rm dc} + \frac{v_{\rm dc}^2}{2R_L}. \end{aligned} \tag{27}$$

To verify whether it is an energy function of the system, partial derivative calculation can be used

$$\frac{\partial P(i,v)}{\partial v_{\rm dc}} = -i_o + \frac{v_{\rm dc}}{R_L} = -C\frac{dv_{\rm dc}}{dt} \tag{28}$$

$$\frac{\partial P(i,v)}{\partial i_{\rm gd}} = v_{\rm gd} - v_{\rm kd} - (R_g+R_s)i_{\rm gd} = (L_g+L)\frac{di_{\rm gd}}{dt}. \tag{29}$$

It can be found that this function $P(i,v)$ not only has the format of a Lyapunov energy function, but also provides a clear physical meaning of each element.

For a mixed-potential function, it has a unified form given by

$$P(i,v) = -A(i) + B(v) + (i, \gamma v - \alpha). \tag{30}$$

Then, the current potential function of nonstorage elements can be found as well as its second-order partial derivative:

$$A(i) = -(v_{\rm gd}-v_{\rm kd})i_{\rm gd} + \frac{(R_g+R_s)i_{\rm gd}^2}{2} \tag{31}$$

$$A_{\rm ii}(i) = \frac{\partial^2 A(i)}{\partial i_{\rm gd}^2} = R_g + R_s. \tag{32}$$

The voltage potential function and its second-order partial derivative can be calculated from (5), (10), and (11), i.e.,

$$B(v) = \int_0^{v_{\rm dc}} i_o dv_{\rm dc} + \frac{v_{\rm dc}^2}{2R_L} \tag{33}$$

$$\begin{aligned} B_{\rm vv}(v) &= \frac{\partial^2 B(v)}{\partial v_{\rm dc}^2} \\ &= -\frac{3I_{d,\rm ref}\left(\frac{L+L_g}{L}k_{\rm vp}k_{\rm ip}V_{\rm dc,ref} - v_{\rm gd} + (R_g+R_s)I_{d,\rm ref}\right)}{2V_{\rm dc,ref}^2} \\ &\quad + \frac{1}{R_L}. \end{aligned} \tag{34}$$

Applying the third theorem of mixed-potential theory, the minimum eigenvalues of $L^{-1/2}A_{\rm ii}(i)L^{-1/2}$ and

$C^{-1/2}B_{\rm vv}(v)C^{-1/2}$ are

$$\mu_1 = \frac{(R_g + R_s)}{L_g + L} \tag{35}$$

$$\mu_2 = -\frac{3I_{d,\rm ref}\left(\frac{L_g+L}{L}k_{\rm vp}k_{\rm ip}V_{\rm dc,ref} - v_{\rm gd} + (R_g+R_s)I_{d,\rm ref}\right)}{2CV_{\rm dc,ref}^2} + \frac{1}{CR_L}. \tag{36}$$

In the grid-connected three-phase VSC system, we have $\mu_1 + \mu_2 > 0$ and when $|i_{\rm gd}| + |v_{\rm dc}| \longrightarrow \infty$, we have

$$P^*(i,v) = (\frac{\mu_1 - \mu_2}{2})P(i,v) + \frac{1}{2}(P_i, L^{-1}P_i) + \frac{1}{2}(P_v, C^{-1}P_v) \longrightarrow \infty \tag{37}$$

and the system will be stable.

Assuming $\mu_1 + \mu_2 > 0$, the large-signal stability criterion can be written as

$$\frac{R_g + R_s}{L_g + L} - \frac{3I_{d,\rm ref}\left(\frac{(L_g+L)k_{\rm vp}k_{\rm ip}V_{\rm dc,ref}}{L} - v_{\rm gd} + (R_g+R_s)I_{d,\rm ref}\right)}{2CV_{\rm dc,ref}^2} + \frac{1}{CR_L} > 0 \tag{38}$$

where $I_{d,\rm ref}$ is the current in the $d$-axis when the VSC is at the operating (equilibrium) point. Clearly, this criterion is from the Lyapunov stability point of view, however, the system should also operate in compliance with power balance, i.e.,

$$P_{\rm load} < \frac{3}{2}(v_{\rm gd}i_{\rm gd} - (R_g + R_s)i_{\rm gd}^2). \tag{39}$$

Thus, the large-signal stability criterion of the three-phase VSC are (38) and (39). For ease of visualization, the stability regions are shown in two-dimensional (2-D) planes. Here, several key parameters that affect the system stability are chosen to illustrate the stability boundaries.

In Fig. 11, the dc-link capacitor $C$, the power rating of the converter $P$, the line reactor including grid impedance $L + L_g$, the parasitic resistance $R_g + R_s$, and the dc-gain of the control loop $k_{\rm vp}$ are investigated. The large-signal stability boundaries are developed for these parameters and presented in 2-D planes. Moreover, we find that this large-signal stability criterion is conservative. When applied to practical system design, the conservative criterion will ensure a reliable system parameter selection.

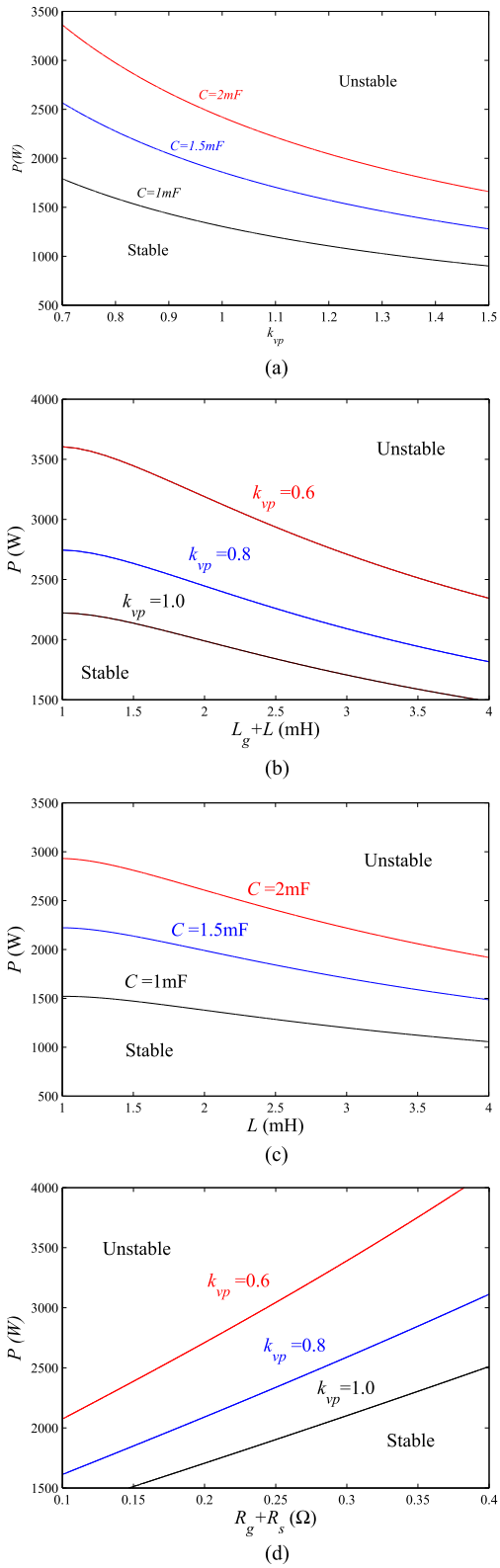


Fig. 11. Stable regions of the grid-connected system derived from the Lyapunov large-signal stability criterion. (a) Calculated stable regions in $P$–$k_{\rm vp}$-plane for different values of dc-link capacitor; (b) calculated stable regions in $P$–$L$-plane for different values of dc gain of the voltage loop; (c) calculated stable regions in $P$–$L$-plane for different values of dc link capacitor; (d) calculated stable regions in $P$–$R$-plane for different values of dc gain of the voltage loop.

## IV. Simulation and Experimental Verification

Following the analysis above, a step change on the grid voltage is applied in transient simulations using a ramp ac voltage, which often occurs in practical grid faults. The grid voltage will step down to 40% of its normal value, and the ramping process lasts for 100 ms. Simulations are performed in MATLAB

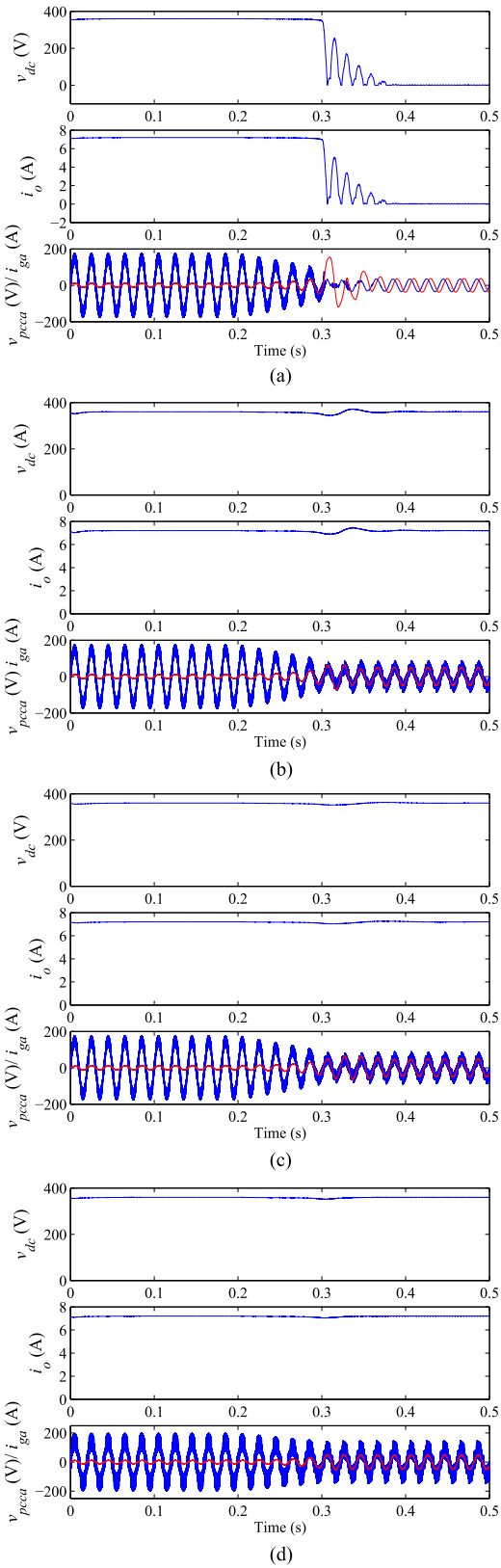


Fig. 12. Simulations for large-signal stability of grid-connected three-phase VSC system. (a) Unstable operation with grid voltage dip leading to catastrophic bifurcation; (b) stable operation with same dip and $k_{\mathrm{vp}} = 1$; (c) stable operation with same dip and $C = 4.5$ mF; (d) stable operation with same dip and $L = 0.1$ mH.

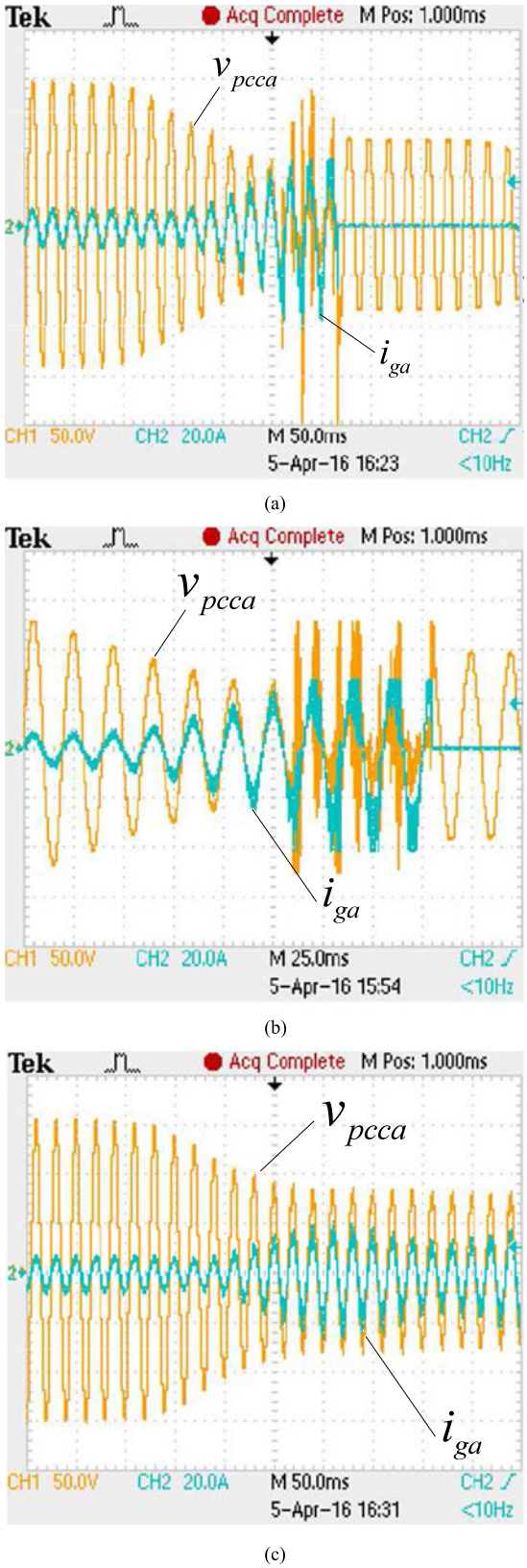


Fig. 13. Experimental verification of large-signal stability of grid-connected three-phase VSC system. (a) Unstable operation with grid voltage dip leading to catastrophic bifurcation; (b) enlarged waveform of (a); (c) stable operation with same dip and a reduced dc gain of the voltage loop.

Simulink with cycle-by-cycle switching models. The system parameters are as listed in Table I.

The results are summarized in Fig. 12. As shown in Section III-B, the system would be unstable if the voltage dip severity goes beyond 49%. In Fig. 12(a), a grid voltage dip of 40% is applied to the grid-connected converter system. Due to the presence of parasitic resistance, no low-frequency oscillation is observed and the system will diverge toward the catastrophic bifurcation boundary. After the disturbance, the system is found to exhibit a catastrophic bifurcation and enter an abnormal operating region. Therefore, the system parameters can be tuned to extend the stable regions, as shown in Fig. 12(a)–(d).

1) As shown in Fig. 12(a), a grid voltage dip occurs at 0.2 s. At 0.3 s, the grid voltage drops to 40% of its normal value, the system exhibits a catastrophic bifurcation after the large disturbance. The ac line current expands and is no longer in-phase with the grid voltage.
2) As shown in Fig. 12(b), when the dc-link capacitance is increased to $k_{\rm vp} = 1$, the system is stable under the same large disturbance. However, the transient response of the system is degraded. There is a fluctuation of $\pm$ 20 V on the dc-link voltage.
3) As shown in Fig. 12(c), when the dc-link capacitance is increased to $C = 4.5$ mF, the system is stable under the same large disturbance. However, the transient response of the system is degraded.
4) As shown in Fig. 12(d), when the line reactor inductance is reduced to $L = 0.1$ mH, the system is stable with the same large disturbance. However, a large amount of harmonics emerges from the ac voltage at the point of common coupling. It may affect the phase-locked-loop of the VSC and cause oscillations.

The stability of the three-phase VSC under grid voltage dips has been verified experimentally. The prototype built in the laboratory is connected to a 110-V ac grid and has a 360-V dc output. However, for practical purposes, a protection mechanism is applied such that the system would be shut down when the peak value of the ac line current is larger than 30 A. The grid voltage drops to 45% of its normal value and the ramp process is about 100 ms. The grid voltage at the point of common coupling is filtered for clarity of presentation. As shown in Fig. 13(a), the ac current in the system expands upon application of a voltage dip. The current stress on the power switches is increased dramatically. When the current amplitude is large enough, the protection mechanism will be triggered to shut down the system. Fig. 13(b) shows the catastrophic bifurcation. In Fig. 13(c), the dc gain of the voltage control loop is reduced, and the system becomes stable after the disturbance.

## V. Conclusion

In this paper, the identification of bifurcation phenomena and large-signal stability analysis of the three-phase VSC under practical grid voltage dip faults are performed. The converter exhibits the catastrophic bifurcation after a large-signal disturbance from the ac side is applied, and the system cannot be restored to its normal operating mode. A bifurcation analysis is adopted to reveal the physical origin of the phenomenon. A Lyapunov large-signal stability analysis is performed based on the mixed-potential theory. A large-signal stability criterion is derived from Lyapunov stability and power balance consideration. Stable regions are identified and presented in 2-D planes involving some key circuit and control parameters. The bifurcation phenomenon and instability are verified by cycle-by-cycle simulations and experimental measurements.

The state equation of the system $\dot{x} = f(x, y, u)$ can be arranged as follows:

$$\begin{cases} f_1(i_{\rm gd}) &= \dfrac{di_{\rm gd}}{dt} = \dfrac{k_{\rm ip}(i_{d,\rm ref} - i_{\rm gd}) + k_{\rm ii}x_2 - R_s i_{\rm gd}}{L} \\ f_2(i_{\rm gq}) &= \dfrac{di_{\rm gq}}{dt} = \dfrac{k_{\rm ip}(i_{q,\rm ref} - i_{\rm gq}) + k_{\rm ii}x_3 - R_s i_{\rm gq}}{L} \\ f_3(v_{\rm dc}) &= \dfrac{dv_{\rm dc}}{dt} = \dfrac{3}{2Cv_{\rm dc}}(v_{\rm kd}i_{\rm gd} + v_{\rm kq}i_{\rm gq}) - \dfrac{v_{\rm dc}}{R_L} \\ f_4(x_1) &= \dfrac{dx_1}{dt} = V_{\rm dc,ref} - v_{\rm dc} \\ f_5(x_2) &= \dfrac{dx_2}{dt} = i_{d,\rm ref} - i_{\rm gd} \\ f_6(x_3) &= \dfrac{dx_3}{dt} = I_{q,\rm ref} - i_{\rm gq}. \end{cases} \tag{40}$$

The control equation $y = g(x, u)$ can be found from (10) and (11), and can be arranged as follows:

$$\begin{cases} g_1(i_{\rm gd}) &= v_{\rm gd} - R_g i_{\rm gd} + \dfrac{L_g}{L}R_s i_{\rm gd} \\ &\quad + \dfrac{L_g + L}{L}(\omega L i_{\rm gq} - k_{\rm ip}(i_{d,\rm ref} - i_{\rm gd}) - k_{\rm ii}x_2) \\ g_2(i_q) &= v_{\rm gq} - R_g i_{\rm gq} + \dfrac{L_g}{L}R_s i_{\rm gq} \\ &\quad + \dfrac{L_g + L}{L}(-\omega L i_{\rm gd} - k_{\rm ip}(I_{q,\rm ref} - i_{\rm gq}) - k_{\rm ii}x_3). \end{cases} \tag{41}$$

The Jacobian $J(X_Q) = A$ is a 6-dim square matrix given by

$$A = \begin{vmatrix} \dfrac{-(R_s + k_{\rm ip})}{L} & 0 & \dfrac{-k_{\rm ip}k_{\rm vp}}{L} & \dfrac{k_{\rm ip}k_{\rm ii}}{L} & \dfrac{k_{\rm ii}}{L} & 0 \\ 0 & \dfrac{-(R_s + k_{\rm ip})}{L} & 0 & 0 & 0 & \dfrac{k_{\rm ii}}{L} \\ J_{31} & 0 & J_{33} & J_{34} & J_{35} & 0 \\ 0 & 0 & -1 & 0 & 0 & 0 \\ 0 & -1 & 0 & 0 & 0 & 0 \end{vmatrix} \tag{42}$$

$$J_{31} = \frac{3(v_{\rm gd} - 2R_g(i_{d,\rm ref} - \frac{L-L_g}{L}R_s i_{d,\rm ref} + \frac{L_g+L}{L}k_{\rm ip}i_{d,\rm ref})}{2CV_{\rm dc,ref}} \tag{43}$$

$$J_{33} = \frac{3i_{d,\mathrm{ref}}\left(\frac{L_g+L}{L}k_{\mathrm{ip}}k_{\mathrm{vp}}V_{\mathrm{dc,ref}} - v_{\mathrm{gd}} + R_g i_{d,\mathrm{ref}} + R_s i_{d,\mathrm{ref}}\right)}{2CV_{\mathrm{dc,ref}}^2} - \frac{1}{R_L C} \tag{44}$$

$$J_{34} = -\frac{3\frac{L_g+L}{L}k_{\mathrm{ip}}k_{\mathrm{vp}}i_{d,\mathrm{ref}}}{2CV_{\mathrm{dc,ref}}} \tag{45}$$

$$J_{35} = \frac{3\frac{L_g+L}{L}k_{\mathrm{ii}}i_{d,\mathrm{ref}}}{2CV_{\mathrm{dc,ref}}}. \tag{46}$$

## REFERENCES


[1] V. Kaura and V. Blasko, "A new method to extend linearity of a sinusoidal PWM in the overmodulation region," *IEEE Trans. Ind. Appl.*, vol. 32, no. 5, pp. 1115–1121, Sep./Oct. 1996.

[2] M. Liserre, F. Blaabjerg, and S. Hansen, "Design and control of an LCL-filter-based three-phase active rectifier," *IEEE Trans. Ind. Appl.*, vol. 41, no. 5, pp. 1281–1291, May 2005.

[3] K. Ma, W. Chen, M. Liserre, and F. Blaabjerg, "Power controllability of a three-phase converter with an unbalanced AC source," *IEEE Trans. Power Electron.*, vol. 30, no. 3, pp. 1591–1604, Mar. 2015.

[4] M. Huang, C. K. Tse, S.-C. Wong, C. Wan, and X. Ruan, "Low-frequency Hopf bifurcation and its effects on stability margin in three-phase PFC power supplies connected to non-ideal power grid," *IEEE Trans. Circuits Syst. I, Reg. Papers*, vol. 60, no. 12, pp. 3328–3340, Dec. 2013.

[5] M. Huang, S.-C. Wong, C. K. Tse, and X. Ruan, "Catastrophic bifurcation in three-phase voltage-source converters," *IEEE Trans. Circuits Syst. I, Reg. Papers*, vol. 60, no. 4, pp. 1062–1071, Apr. 2013.

[6] M. Zamani, A. Yazdani, and T. Sidhu, "A control strategy for enhanced operation of inverter-based microgrids under transient disturbances and network faults," *IEEE Trans. Power Del.*, vol. 27, no. 4, pp. 1737–1747, Apr. 2012.

[7] X. Guo, X. Zhang, B. Wang, W. Wu, and J. M. Guerrero, "Asymmetrical grid fault ride-through strategy of three-phase grid-connected inverter considering network impedance impact in low-voltage grid," *IEEE Trans. Power Electron.*, vol. 29, no. 3, pp. 1064–1068, Mar. 2014.

[8] K. Jalili and S. Bernet, "Design of filters of active-front-end two-level voltage-source converters," *IEEE Trans. Ind. Electron.*, vol. 56, no. 5, pp. 1674–1689, May 2009.

[9] Y. Tang, P. C. Loh, P. Wang, F. H. Choo, F. Gao, and F. Blaabjerg, "Generalized design of high performance shunt active power filter with output LCL filter," *IEEE Trans. Ind. Electron.*, vol. 59, no. 3, pp. 1443–1452, Mar. 2012.

[10] J. Sun, "Small-signal methods for AC distributed power systems a review," *IEEE Trans. Power Electron.*, vol. 24, no. 11, pp. 2545–2554, Nov. 2009.

[11] J. Sun, "Impedance-based stability criterion for grid-connected inverters," *IEEE Trans. Power Electron.*, vol. 26, no. 11, pp. 3075–3078, Nov. 2011.

[12] I. Erlich, H. Wrede, and C. Feltes, "Dynamic behavior of DFIG-based wind turbines during grid faults," in *Proc. Power Convers. Conf.*, Apr. 2007, pp. 1195–1200.

[13] A. Junyent-Ferre, O. Gomis-Bellmunt, T. Green, and D. Soto-Sanchez, "Current control reference calculation issues for the operation of renewable source grid interface VSCs under unbalanced voltage sags," *IEEE Trans. Power Electron.*, vol. 26, no. 12, pp. 3744–3753, Dec. 2011.

[14] J. Miret, M. Castilla, A. Camacho, L. Garca de Vicura, and J. Matas, "Control scheme for photovoltaic three-phase inverters to minimize peak currents during unbalanced grid-voltage sags," *IEEE Trans. Power Electron.*, vol. 27, no. 10, pp. 4262–4271, Oct. 2012.

[15] H. H. C. Iu and C. K. Tse, "Study of low-frequency bifurcation phenomena of a parallel-connected boost converter system via simple averaged models," *IEEE Trans. Circuits Syst. I, Fund. Theory Appl.*, vol. 50, no. 5, pp. 679–685, May 2003.

[16] X. Xiong, C. K. Tse, and X. Ruan, "Bifurcation analysis and experimental study of a multi-operating-mode photovoltaic-battery hybrid power system," *IEEE J. Emerg. Sel. Topics Circuits Syst.*, vol. 5, no. 3, pp. 316–325, Sep. 2015.

[17] L. Benadero, R. Cristiano, D. Pagano, and E. Ponce, "Nonlinear analysis of interconnected power converters: A case study," *IEEE J. Emerg. Sel. Topics Circuits Syst.*, vol. 5, no. 3, pp. 326–335, Sep. 2015.

[18] C. Wan, M. Huang, C. K. Tse, S.-C. Wong, and X. Ruan, "Nonlinear behavior and instability in a three-phase boost rectifier connected to a nonideal power grid with an interacting load," *IEEE Trans. Power Electron.*, vol. 28, no. 7, pp. 3255–3265, Jul. 2013.

[19] W. Du, J. Zhang, Y. Zhang, and Z. Qian, "Stability criterion for cascaded system with constant power load," *IEEE Trans. Power Electron.*, vol. 28, no. 4, pp. 1843–1851, Apr. 2013.

[20] M. Kabalan, P. Singh, and D. Niebur, "Large signal Lyapunov-based stability studies in microgrids: A review," *IEEE Trans. Smart Grid*, vol. PP, no. 99, pp. 1–9.

[21] A. Houari, H. Renaudineau, B. Nahid-Mobarakeh, J. P. Martin, S. Pierfederici, and F. Meibody-Tabar, "Large signal stability analysis and stabilization of converters connected to grid through filters," *IEEE Trans. Ind. Electron.*, vol. 61, no. 12, pp. 6507–6516, Dec. 2014.

[22] Y. Peng *et al.*, "Transient response of three-phase voltage-source converters under grid-side faults," in *Proc. IEEE Energy Convers. Congr. Expo.*, Sep. 2015, pp. 2728–2733.

[23] K. Cheng, S. Ho, K. P. Wong, T. Cheung, and Y. Ho, "Examination of square-wave modulated voltage dip restorer and its harmonics analysis," *IEEE Trans. Energy Convers.*, vol. 21, no. 3, pp. 759–766, Mar. 2006.

[24] M. Bollen, *Understanding Power Quality Problems.* New York, NY, USA: IEEE Press, 2000.

[25] C. K. Tse, *Complex Behavior of Switching Power Converters.* Boca Raton, FL, USA: CRC Press, 2003.

[26] S. Banerjee and G. C. Verghese, Eds.), *Nonlinear Phenomena in Power Electronics.* New York, NY, USA: IEEE Press, 2001.

[27] M. I. Feigin, "Doubling of the oscillation period with C-bifurcations in piecewise continuous systems: PMM," *J. Appl. Math. Mech.*, vol. 34, pp. 861–869, 1970.

[28] M. di Bernardo, C. J. Budd, A. R. Champneys, and P. Kowalczyk, *Bifurcation and Chaos in Piecewise-Smooth Dynamical Systems: Theory and Applications.* London, U.K.: Springer-Verlag, 2008.

[29] H. E. Nusse and J. A. Yorke, "Border-collision bifurcations including 'period two to period three' for piecewise smooth systems," *Physica D*, vol. 57, pp. 39–57, 1992.

[30] G. H. Yuan, S. Banerjee, E. Ott, and J. A. Yorke, "Border-collision bifurcations in the buck converter," *IEEE Trans. Circuits Syst. I, Fundam. Theory Appl.*, vol. 45, no. 7, pp. 707–716, Jul. 1998.

[31] F. Xie, R. Yang, and B. Zhang, "Bifurcation and border collision analysis of voltage-mode-controlled flyback converter based on total ampere-turns," *IEEE Trans. Circuits Syst. I, Reg. Papers*, vol. 58, no. 9, pp. 2269–2280, Sep. 2011.

[32] A. El Aroudi, "A new approach for accurate prediction of subharmonic oscillation in switching regulators—Part I: Mathematical derivations," *IEEE Trans. Power Electron.*, vol. 32, no. 7, pp. 5651–5665, Jul. 2017.

[33] S. Muratori and S. Rinaldi, "Catastrophic bifurcations in a second-order dynamical system with application to acid rain and forest collapse," *Appl. Math. Model.*, vol. 13, no. 12, pp. 674–681, Dec. 1989.

[34] F. Dercole, "Border collision bifurcations in the evolution of mutualistic interactions," *Int. J. Bifurcation Chaos*, vol. 15, no. 7, pp. 2179–2190, Jul. 2005.

[35] R. K. Brayton and J. K. Moser, "A theory of nonlinear networks—I," *Quart. Appl. Math.*, vol. 22, pp. 1–33, Apr. 1964.

[36] X. Liu, Y. Zhou, W. Zhang, and S. Ma, "Stability criteria for constant power loads with multistage LC filters," *IEEE Trans. Veh. Technol.*, vol. 60, no. 5, pp. 2042–2049, Jun. 2011.

[37] M. Belkhayat, R. Cooley, and A. Witulski, "Large signal stability criteria for distributed systems with constant power loads," in *Proc. 26th Annu. IEEE Power Electron. Spec. Conf.*, Jun. 1995, pp. 1333–1338.



**Meng Huang** (S'11–M'13) received the B.Eng. and M.Eng. degrees in electronic science and technology from the Huazhong University of Science and Technology, Wuhan, China, in 2006 and 2008, respectively, and the Ph.D. degree in power electronics from the Hong Kong Polytechnic University, Hong Kong, in 2013.

He is currently an Associate Professor at the School of Electrical Engineering, Wuhan University, Wuhan, China. His research interests include nonlinear analysis of power converters and power electronics reliability.

**Yu Peng** was born in Hubei Province, China, in 1991. She received the B.Eng. and M.Eng. degrees in electrical engineering and its automation from Wuhan University, Wuhan, China, in 2013 and 2016, respectively.

She is currently working in the Wuhan Electric Power Technical College as an Assistant Professor. Her research interests include power electronics and nonlinear analysis.

**Chi K. Tse** (M'90–SM'97–F'06) received the B.Eng. (first class Hons.) degree in electrical engineering and the Ph.D. degree from the University of Melbourne, Melbourne, Vic, Australia, in 1987 and 1991, respectively.

He is currently the Chair Professor at the Hong Kong Polytechnic University, Hong Kong, where he was the Head of the Department of Electronic and Information Engineering from 2005 to 2012. He is the author/coauthor of 10 books, 20 book chapters, and more than 500 papers in research journals and conference proceedings, and holds 5 U.S. patents.

Dr. Tse received a number of research and industry awards, including Prize Paper Awards by the IEEE TRANSACTIONS ON POWER ELECTRONICS in 2001 and 2015, the RISP Journal of Signal Processing Best Paper Award in 2014, the Best paper Award by *International Journal of Circuit Theory and Applications* in 2003, two Gold Medals at the International Inventions Exhibition in Geneva in 2009 and 2013, and a number of recognitions by the academic and research communities, including honorary professorship by several Chinese and Australian universities, the Chang Jiang Scholar Chair Professorship, the IEEE Distinguished Lectureship, the Distinguished Research Fellowship by the University of Calgary, the Gledden Fellowship, and the International Distinguished Professorship-at-Large by the University of Western Australia. While with the Hong Kong Polytechnic University, he received the President's Award for Outstanding Research Performance twice, the Faculty Research Grant Achievement Award twice, the Faculty Best Researcher Award, and several teaching awards. He is the Editor-in-Chief for the IEEE TRANSACTIONS ON CIRCUITS AND SYSTEMS II (2016–2017), IEEE CIRCUITS AND SYSTEMS MAGAZINE (2012–2015), the IEEE CIRCUITS AND SYSTEMS SOCIETY NEWSLETTER (since 2007), the Associate Editor for three IEEE Journal/Transactions, the Editor for *International Journal of Circuit Theory and Applications*, and is on the editorial boards of a few other journals. He is also a panel member of Hong Kong Research Grants Council and NSFC, and a member of several professional and government committees.

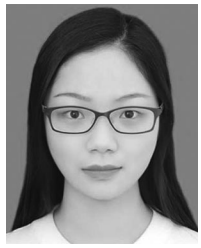

**Yushuang Liu** was born in Hubei, China. She received the B.S. degree in electrical engineering from Wuhan University, Wuhan, China, in 2016, where she is currently working toward the M.S. degree in electrical engineering and its automation.

Her research interests include large-signal stability and nonlinear analysis of power converters.

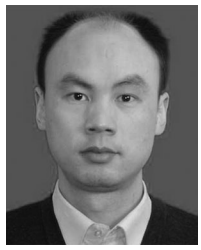

**Jianjun Sun** (M'13) was born in 1975. He received the B.Eng. degree from Wuhan University of Hydraulic and Electrical Engineering, Wuhan, China, in 1997, and the M.Eng. and Ph.D. degrees, all in electrical engineering and its automation from Wuhan University, Wuhan, China, in 2000 and 2007, respectively.

He is currently working in the School of Electrical Engineering, Wuhan University, Wuhan, as an Associate Professor and the Deputy Director of the Motor and Power Electronics Center. His current research interests include modeling and analysis of high-power power-electronic system, operation and control of microgrid, and power quality analysis and compensation.

Dr. Sun is an Associate Director of Wuhan Power Supply Society.

**Xiaoming Zha** (M'02) was born in Huaining, Anhui Province, China, in 1967. He received the B.S., M.S., and Ph.D. degrees in electrical engineering from Wuhan University, Wuhan, China, in 1989, 1992, and 2001, respectively.

From 2001 to 2003, he was a Postdoctoral Fellow with the University of Alberta, Edmonton, AB, Canada. Since 1992, he has been a Faculty Member at Wuhan University, where he became a Professor in 2003. He is currently a Deputy Dean in the School of Electrical Engineering, Wuhan University, Wuhan, China. His research interests include power electronic converter, the application of power electronics in smart grid and renewable energy generation, the analysis and control of microgrid, the analysis and control of power quality, and frequency control of high-voltage high-power electric motors.